ference between their 1-d results and their 2-d results.

The author gratefully acknowledges the support of the Fannie and John Hertz Foundation during much of the course of this research. The comments and assistance of G. B. Field, C. K. Birdsall, A. B. Langdon, and D. L. Book were invaluable.

*Work performed under the auspices of the U. S. Atomic Energy Commission.

[1]R. Z. Sagdeev, in *Reviews of Plasma Physics*, edited by M. A. Leontovich (Consultants Bureau, New York, 1966), Vol. 4, pp. 23-91.

[2]D. Montgomery and G. Joyce, J. Plasma Phys. 3, 1 (1969).

[3]R. J. Taylor, D. R. Baker, and H. Ikezi, Phys. Rev. Letters 24, 206 (1970).

[4]D. A. Tidman, Phys. Fluids 10, 547 (1967).

[5]S. A. Colgate and C. W. Hartman, Phys. Fluids 10, 1288 (1967).

[6]H. Mott-Smith, Phys. Rev. 82, 885 (1951).

[7]T. E. Stringer, Plasma Phys. 6, 267 (1964).

[8]C. Smith and J. Dawson, Princeton Plasma Physics Laboratory Report No. MATT-151 (1963).

[9]C. K. Birdsall, A. B. Langdon, C. F. McKee, H. Okuda, and D. Wong, Bull. Am. Phys. Soc. 13, 1747 (1968).

[10]J. M. Dawson and R. Shanny, Phys. Fluids 11, 1506 (1968).

[11]R. L. Morse and C. W. Nielsen, Phys. Rev. Letters 23, 1087 (1969).

[12]R. C. Davidson, N. A. Krall, K. Papadopoulos, and R. Shanny, Phys. Rev. Letters 24, 579 (1970).

[13]C. R. Shonk and R. L. Morse, in Proceedings of the Third Annual Numerical Plasma Simulation Conference, Stanford, Calif., 1969 (to be published), Paper No. II-10.

[14]M. Lampe, private communication.

[15]J. M. Dawson, K. Papadopoulos, and R. Shanny, to be published.

[16]J. M. Dawson, private communication.

FAST TIME-RESOLVED SPECTRA OF ELECTROSTATIC TURBULENCE IN THE EARTH'S BOW SHOCK*

R. W. Fredricks, F. V. Coroniti,† C. F. Kennel,† and F. L. Scarf
Space Sciences Laboratory, TRW Systems Group, Redondo Beach, California 90278
(Received 2 January 1970)

We present time-resolved spectra of electrostatic turbulence in the earth's bow-shock structure. Spectral details on scales for a few Debye lengths indicate that single modes or groups of single modes dominate the turbulent spectrum. These modes are probably ion-acoustic or Buneman instabilities of short wavelength ($k\lambda_D \sim 1$) which are generated in parts of the shock microstructure containing diamagnetic drift currents.

In a previous note,[1] evidence for the detection of electric field turbulence in the earth's collisionless bow shock was presented. At that time, only narrow-band filter and broad-band frequency-time analyses of this turbulence were available. We have recently subjected the broad-band analog electric field data (1-22 kHz) from our OGO-5 experiment[2] to a fast-time-resolution spectral analysis which allows a complete turbulence spectrum over a selected passband to be formed each 12.5 msec. During a 12.5 msec interval, the spacecraft moves through a distance comparable with the plasma Debye length, or some 20-40 m. Thus the time-resolved spectra allow examination of very fine details of shock turbulence. We have chosen a fairly typical example of such a time-resolved spectrum of turbulence in a bow-shock structure observed near $0^h46^m54^s$ UT on 12 March 1968. We believe that these spectra are the first ever presented showing the microscopic details of electrostatic wave turbulence. As such, they should be of interest not only to the understanding of the collisionless shock dissipation mechanism, but also to the descriptions of plasma turbulence by such tools as quasilinear theory.

In any single satellite measurement, the length scales inferred from measurements must always involve some assumption about the convection of the plasma disturbance relative to the spacecraft. The upstream conditions at the time of shock encounter were approximately: ion density $n \sim 10\ \mathrm{cm}^{-3}$; flow speed $U_0 \sim 380$ km/sec; ion temperature $T_i \sim 6.3 \times 10^4\ ^\circ\mathrm{K}$; electron temperature unknown, but probably $T_e \sim 10^5\ ^\circ\mathrm{K}$; interplanetary field $B_0 \sim 7 \times 10^{-5}$ G; satellite orbital speed $V_s \sim 1.9$ km/sec. From these parameters we conclude $\omega_{pi}/2\pi \sim 650$ Hz, $\omega_{pe}/2\pi \sim 28$ kHz, $c/\omega_{pe} \sim 1.7$ km, $c/\omega_{pi} \sim 73$ km, $\omega_{ce}/2\pi \sim 200$ Hz, $\omega_{ci}/2\pi \sim 0.11$ Hz, and $\lambda_D \sim 7$ m.

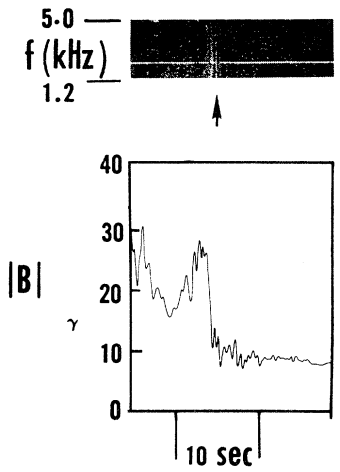

FIG. 1. Dynamic spectrum (frequency versus time, or f-t diagram) of electrostatic turbulence and the total magnetic field profile for the bow shock discussed in text. The arrow points to the portion of turbulence spectrum corresponding to the fast-time-resolved spectra of Fig. 2. The units of $|B|$ are $1\ \gamma = 10^{-5}$ G. The constant-frequency horizontal line in the f-t plot is a 2.461 kHz interference line generated by a spacecraft oscillator.

The spacecraft was inbound towards earth at the time corresponding to Fig. 1. Thus, the spacecraft was immersed in the downstream region (so-called "magnetosheath") and the shock structure swept over it, leaving the spacecraft behind in the upstream region (solar wind). In the earth's inertial frame, the earthward speed of the shock front was necessarily greater than the earthward speed of the satellite. Based on experimental estimates[3,4] of bow-shock speeds, it is not unreasonable to use an estimate of 10 km/sec for the relative shock-satellite speed (i.e., an earthward shock speed of ~12 km/sec).

Figure 1 presents the total magnetic field profile and a time-correlated dynamic spectrum of electric field fluctuations through the shock in question. In Fig. 1, the upstream region is on the right side, and downstream on the left, with the entire plot covering about 26 sec in time. Note the very sharp magnetic field gradient and its correlation with the electric field fluctuations in the f-t plot, a feature previously pointed out.[1] Figure 2 is the time-resolved spectrum of the electric field turbulence between 1.2 and 2.2 kHz over a time interval of about 500 msec in the neighborhood indicated by the arrow in Fig. 1. The spectra of Fig. 2 are the output of a logarithmic amplifier; hence, the spectral amplitudes are nonlinear, with large-amplitude fluctuations compressed and small ones enhanced. The entire turbulence spectrum in this shock front has been so analyzed, but the main features are fairly well typified by the short segment in Fig. 2.

Some important qualitative features of the electrostatic wave turbulence can be extracted from spectra such as that in Fig. 2. For example, under the assumption that the satellite (measurement frame) moves at ~10 km/sec relative to the rest (shock structure) frame, we note that the turbulence builds up as a set of a few single frequencies (or modes) in about 4 to 5 spectral sweeps, i.e., in some 50 Debye lengths, after which many more frequencies are excited. Also, in this region, the linewidths are some 25 to 75 Hz. The electric field at 1.3 ± 0.1 kHz was measured by a digital channel and found to be about 1 mV/m, for the spectral peak at that frequency in Fig. 2.

The spectral analysis shown in Fig. 2 was performed with a Federal Scientific Corporation

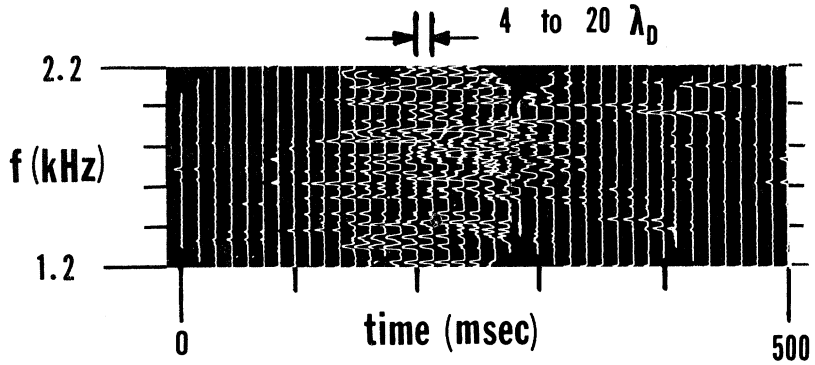

FIG. 2. Fast-time-resolved spectrum of a portion of the electrostatic turbulence in the bow shock of Fig. 1. Each spectral sweep is performed in 12.5 msec. The length scale shown at the top of the figure corresponds to either the distance traveled by the spacecraft ($4\lambda_D$) or the distance traveled by a 10 km/sec shock front ($20\lambda_D$) during 12.5 msec. Details are discussed in the text.

model UA-6 spectrum analyzer. The original data tapes containing the waveform $f(t)$ were played back at $\frac{1}{4}$ speed, thus reducing the frequencies in $f(t)$ by the same factor. The analyzer was then set to the passband 300-550 Hz, equivalent to the band 1.2-2.2 kHz for the real-time signal $f(t)$. The display time was set to 25 msec, equivalent to $25/4 = 6.25$ msec in real time. Every other spectral sweep (i.e., $6.25 \times 2 = 12.5$ msec) was then used to produce Fig. 2. The length of signal used in "decelerated time" processing by the UA-6 analyzer was $T = 1$ sec, equivalent to 250 msec in tape real time. Under these conditions the maximum resolution of real-time signals is $\Delta f \sim 1/0.25 = 4$ Hz, which would be achieved provided the frequency component ω_k was produced by a portion of $f(t)$ persisting at least for 250 msec. If the ω_k component persists for $\tau_D < T = 250$ msec, the maximum possible resolution is $\Delta f \sim \tau_D^{-1}$.

In order to determine the "transient" features of the swept spectra produced by the UA-6 analyzer, a set of truncated sinusoidal tone bursts with duration $\tau_D <$ analyzer resolving time (1 sec for upper cutoff of 500 Hz) and frequency $f_0 \gg \tau_D^{-1}$ was analyzed. The results of these tests are shown in Fig. 3. If the signal input to the UA-6 analyzer does not overload its digital circuits (i.e., no pile-up) the results shown in Fig. 3 are independent of signal amplitude, a condition always maintained in our signal processing. The short tone bursts containing only 8 or 16 periods of the 250 Hz sinusoid (equivalent to 1 kHz in Fig. 2) are poorly resolved. The plot of the duration of the UA-6 spectral output against the duration of the input tone burst shows that as the duration of the pulsed sinusoid increases beyond 250 msec, or one-fourth the analyzer resolving time of 1 sec, the two durations become equal.

To convert the scales of Fig. 3 to those of Fig. 2, one simply divides times by, or multiplies frequencies by, a factor of 4.

A frequently observed characteristic of the electrostatic turbulence is that of apparent break-up of the largest amplitude, broadest peaks into several discrete peaks, or single modes. Some such behavior is apparent in Fig. 2, although many better examples have been found in other spectral displays for the same shock. However, caution is required in making such an interpretation. As noted above, the resolution of closely spaced peaks may be relatively poor during the first two or three sweeps after initial appearance, then improve in later sweeps because a greater segment of $f(t)$ enters the processing of $F(\omega)$. Also, instrumental broadening of the peaks of $F(\omega)$ can occur if the signal $f(t)$ has components $\omega_k(t)$ for which $\omega_k(t_0) - \omega_k(t_0 + \tau_D) \gtrsim 2\pi/T$. This frequency modulation effect may be involved in the broadened spectra between 1.8 and 2.0 kHz in Fig. 2.

The spectra in Fig. 2 must be Doppler shifted, at least by the relative motion between shock structure and satellite, and at most by the solar wind speed. It is a noteworthy feature of Fig. 2 that the turbulent energy appears in sensibly discrete frequency bands whose center frequencies do not shift appreciably during their persistence time. These center frequencies, ω, are related to the rest frame frequency ω_0 by $\omega = \omega_0 \pm |\vec{k} \cdot \vec{V}|$. Because of the correlation of regions of electrostatic turbulence with magnetic field gradients having scale lengths $\sim c/\omega_{pe}$, a fact pointed out previously,[1] we expect $\omega_0 \gtrsim \omega_{pi}$, i.e., the turbulence is assumed to be due to either an ion-acoustic or Buneman[5] instability. Then we would expect its $\vec{k}$ spectrum to peak near $k\lambda_D \sim 1$, with $\vec{k}$ in the Čerenkov cone peaked in the direction of

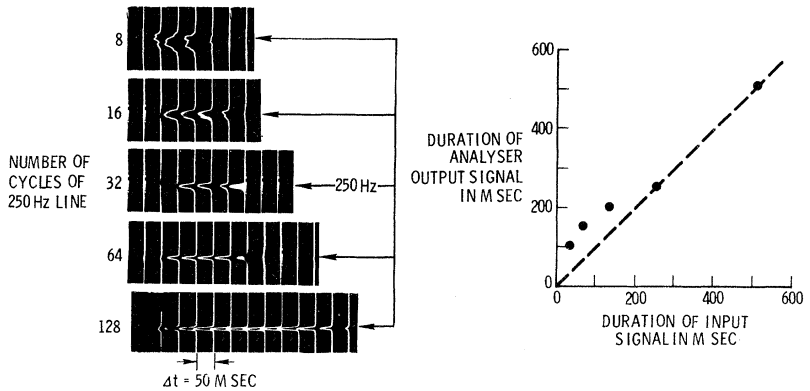

FIG. 3. Time response of spectrum analyzer to truncated sinusoidal signals of various durations at 250 Hz. Time-resolved spectra are shown at the left, with duration of spectrum against pulse duration at right.

the current that drives the instability.[6] Under such assumptions the center frequency would occur at

$$\omega = \omega_0 + V\lambda_D^{-1}|\cos\theta|,$$

where

$$|\vec{k}\cdot\vec{V}| = kV|\cos\theta|.$$

The Doppler-shift contribution to ω, when we assume $\vec{V}$ is the shock speed of ~10 km/sec, is

$$\Delta\omega = V\lambda_D^{-1}|\cos\theta| \lesssim (10^3\ \mathrm{sec}^{-1})|\cos\theta|,$$

or

$$\Delta f \lesssim (160\ \mathrm{Hz})|\cos\theta|.$$

However, if $V|\cos\theta|$ is interpreted as the projection of the solar wind flow speed along $\vec{k}$, the shift could be as much as

$$\Delta f \lesssim (6\ \mathrm{kHz})|\cos\theta| \sim 6\ \mathrm{kHz},$$

for $|\cos\theta| \simeq 1$. Because the electrostatic turbulence in Fig. 1 appears in such a broad frequency band (up to about 4 kHz), we favor the latter explanation. Thus, we picture the process as follows. The region of strong diamagnetic current density $\vec{J} \sim (c/4\pi)\Delta\vec{B}/\Delta\vec{x}$ moves with the relative shock speed. In this region, wave turbulence is continuously generated, and these waves are blown by the solar wind flow at speed $U_0\cos\theta$ along $\vec{k}$ (roughly along $\vec{J}$) and out of the current layer at speed $U_0\sin\theta$ (perpendicular to $\vec{J}$). As they leave the current layer by the latter process they rapidly decay due to Landau or other damping mechanisms (with their energy reappearing as partial randomization of particle speeds). This is the most reasonable picture of the electrostatic turbulence that conforms to the observed frequency spread and location within the magnetic field profile.

Unfortunately, the linewidths of the spectra in Fig. 2 cannot be interpreted in terms of natural widths γ_k of growing modes at frequencies ω_k. The best one can do is to measure the time of persistence τ_D' of a given peak, form $\Delta f' = (\tau_D')^{-1}$, and compare this derived quantity with the observed linewidth Δf. In Fig. 2, all lines have the property $\Delta f \gtrsim \Delta f'$, which could be interpreted as evidence for truncated sinusoidal (tone-burst) signals.

Our speculations based on these preliminary studies of fast time-resolved spectra are summarized as follows:

(1) It appears that the microinstabilities observed here are basically electrostatic modes excited by diamagnetic currents in the shock structure. These begin as weak single modes with narrow frequency distributions. As the instability strengthens, the number of single modes excited increases.

(2) The center frequencies of these modes are most likely ion-acoustic (ω_{pi}) or Buneman ($0.08\omega_{pe}$) modes with Doppler shifts of up to several kHz. This observed span of Doppler shifting can best be explained by short wavelength ($k\lambda_D \sim 1$) modes blown along $\vec{k}$ by the projection of flow speed in that direction, and out of their region of generation by the flow speed normal to $\vec{k}$.

(3) Even when the turbulence becomes quite strong in the sense that $\sum_j \langle E^2\rangle_j/8\pi nkT_e \gtrsim 10^{-2}$ (sum over all observed excited modes), the spectral form of the turbulence contains strong single mode peaks. Averaged over several successive spectra, the wave turbulence remains dominated by these single modes, and is not the broad smooth spectrum over many ω_k values usually assumed in a quasilinear theory. We believe that the observed spectra, even though consisting largely of resolved ω_k's, would still yield averages of $\vec{E}_k$ on quasilinear time scales which would in turn permit the usual quasilinear reconstruction of the distribution function by total diffusion due to the sum of all resolved modes. However, quasilinear descriptions of the spectrum are not consistent with the resolved modes shown in Fig. 2.

(4) A relationship of the electrostatic turbulence to proton randomization is experimentally observed. The proton thermalization occurs only after the flow has traversed a region of strong turbulence in which many modes (ω_k's) are excited simultaneously and persist for measured times of up to a few seconds (corresponding to scale lengths $\sim c/\omega_{pe}$). Thus, we speculate that the multiple scattering of ions by these many single modes may be a very significant dissipative process in this type of collisionless shock.

We are indebted to A. Belobradic for providing techniques leading to the fast time-resolved spectra shown here; to P. J. Coleman, Jr., and C. T. Russell for the University of California at Los Angeles fluxgate magnetometer data shown in Fig. 1; and to M. Neugebauer of the Jet Propulsion Laboratory for plasma probe measurements of upstream density, temperature, and flow velocity.

*Work supported by NASA through the Orbiting Geophysical Observatory Project Office, Goddard Space

Flight Center, under Contract No. NAS 5-9278.

†Permanent address: Department of Physics, University of California, Los Angeles, Calif. 90024.

[1]R. W. Fredricks, C. F. Kennel, F. L. Scarf, G. M. Crook, and I. M. Green, Phys. Rev. Letters 21, 1761 (1968).

[2]G. M. Crook *et al.*, IEEE Trans. Geosci. Electron. 7, 120 (1969).

[3]R. E. Holzer *et al.*, J. Geophys. Res. 71, 1481 (1966).

[4]J. P. Heppner *et al.*, J. Geophys. Res. 72, 5417 (1967).

[5]O. Buneman, Phys. Rev. Letters 1, 8 (1958).

[6]B. B. Kadomtsev, *Plasma Turbulence* (Academic, New York, 1965).

EVOLUTION FROM LINEAR TO NONLINEAR SATURATION OF INSTABILITIES AND CHANGE IN ZEROTH-ORDER CONDITIONS

Masumi Sato

Department of Electrical Engineering, Yamagata University, Yonezawa, Japan

(Received 5 March 1970)

An evolution from the linear growth to the nonlinear saturated state of instability is investigated by observing the spatially growing ionization waves (moving striations) in a plasma. The behavior of the instability is shown to obey the Landau amplitude equation. Partial, gradual change in zeroth-order conditions by the nonlinear effect is also found.

We report an experimental observation of both the evolution to the nonlinear saturation of the spatially unstable mode and the change in the zeroth-order conditions. Recently, Wong and Hai[1] suggested that their method of measuring growth rates of temporally unstable modes can be also applied to the case of spatially unstable modes which saturate at a certain distance. The behavior of such modes can be represented by the Landau amplitude equation[2]

$$d|A|^2/dx = 2\gamma|A|^2 - \alpha|A|^4 - \beta|A|^6, \quad (1)$$

where $|A|$ represents the magnitude of the wave amplitude, γ the linear growth rate, α and β the first and second nonlinear saturation coefficients, and higher-order terms are neglected. From (1), $|A|$ is obtained as

$$\frac{|A|^2}{|A_1|^2} = \frac{\exp[2\gamma(x-x_1)]}{1-(|A_1|/|A_2|)^2\{1-\exp[2\gamma(x-x_1)]\}}, \quad (2)$$

where $|A| = |A_1|$ at $x = x_1$, $|A| = |A_2|$ at large x, and an assumption $\alpha^2 > 8\beta\gamma$, which can be easily satisfied,[1] is used. When $2\gamma(x-x_1) \simeq 0$, the mode grows exponentially: $|A| = |A_1| \exp[\gamma(x-x_1)]$. When $2\gamma(x-x_1) \gg 1$, it reaches a saturated or equilibrium amplitude

$$|A_2|^2 = [(\alpha^2 + 8\beta\gamma)^{1/2}\alpha]/2\beta \simeq 2\gamma/\alpha. \quad (3)$$

This value is independent of the initial infinitesimal amplitude $|A_1|$, and returns to the same amplitude even if the saturated state is perturbed by an external disturbance. First we observe the behavior of the nonlinear saturation by considering the case of an ionization-wave mode in positive columns.

The ionization wave (moving striation)[3] is a low-frequency oscillation appearing as the result of change of ionization and usually exists as a backward wave for discharge currents below an upper critical current, the so-called Pupp current. As the critical current is approached, the ionization wave does not simultaneously disappear throughout the discharge but first vanishes in the cathode region of the positive column and then, as the current is further increased, the region of zero mode extends further toward the anode. Under these conditions the amplitude of the ionization wave increases from the region of zero mode (cathode) towards the anode. These features allow systematic studies of a spatially growing mode. As the signal of the oscillation is fed back from the anode to the cathode through the external circuit,[3] we controlled the initial amplitude of the unstable mode by using a circuit shown in Fig. 1(a). The signal picked up by a transformer is amplified and then fed back to a current modulator, in phase or out of phase by changing polarity, so that the initial amplitude can be easily either enhanced or suppressed. In addition to this method, the nonlinear equilibrium was also perturbed by means of a local transverse magnetic field $B \sim 150$ G. Light intensities of the mode were measured by a phototransistor, movable along the tube, as a function of distance x from the cathode. The solid lines in Fig. 1(b) represent variation of the amplitude controlled

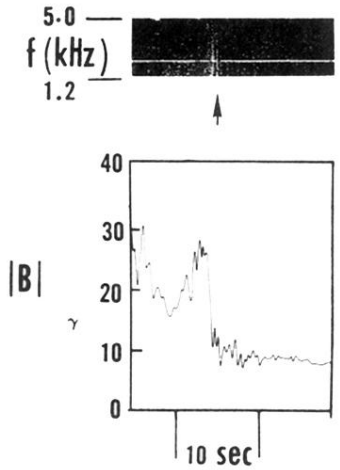

FIG. 1. Dynamic spectrum (frequency versus time, or f–t diagram) of electrostatic turbulence and the total magnetic field profile for the bow shock discussed in text. The arrow points to the portion of turbulence spectrum corresponding to the fast–time-resolved spectra of Fig. 2. The units of $|B|$ are $1\ \gamma = 10^{-5}$ G. The constant-frequency horizontal line in the f–t plot is a 2.461 kHz interference line generated by a spacecraft oscillator.

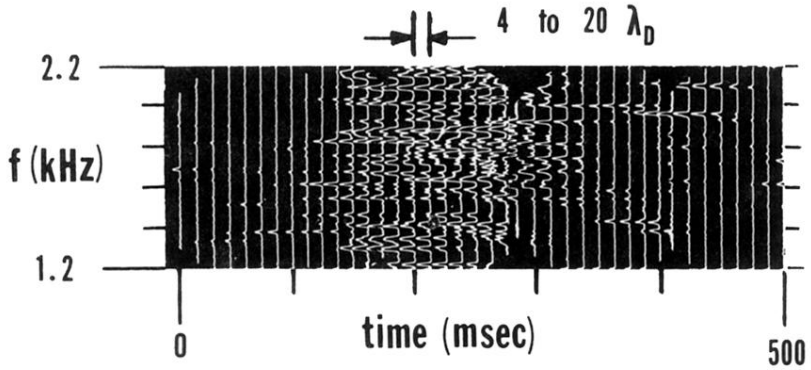

FIG. 2. Fast–time-resolved spectrum of a portion of the electrostatic turbulence in the bow shock of Fig. 1. Each spectral sweep is performed in 12.5 msec. The length scale shown at the top of the figure corresponds to either the distance traveled by the spacecraft ($4\lambda_D$) or the distance traveled by a 10 km/sec shock front ($20\lambda_D$) during 12.5 msec. Details are discussed in the text.

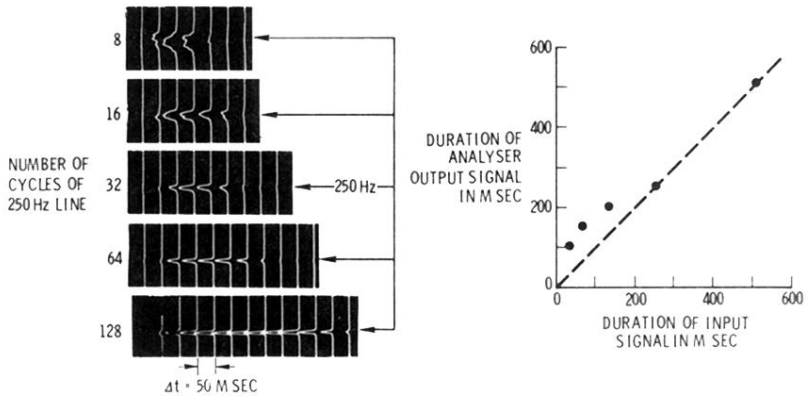

FIG. 3. Time response of spectrum analyzer to truncated sinusoidal signals of various durations at 250 Hz. Time-resolved spectra are shown at the left, with duration of spectrum against pulse duration at right.